Supporting information

MnO Nanoparticles with Cationic Vacancies and Discrepant Crystallinity Dispersed into Porous Carbon as Anode for Li ion Pseudocapacitors

Chaofeng Liu, Changkun Zhang, Huanqiao Song, Xihui Nan, Haoyu Fu and Guozhong Cao

Figure S1a shows the XRD pattern of the resulting sample synthesized using hydrothermal growth without any calcination treatment. All characteristic peaks can be indexed to $MnCO_3$ (R-3C, PDF 44-1472), indicating that $KMnO_4$ (Mn^{7+}) reacted with glucose, and together with $Mn(CH_3COO)_2{\cdot}4H_2O$ (Mn^{2+}) to produce Mn(II)-compound during the hydrothermal treatment. Fourier Translation Infrared Spectroscopy (FT-IR) was used to analyze the functional groups in the resulting product (Figure S1b). The characteristic peaks at 1448 and 862 cm^{-1} derived from the CO_3^{2-} vibrations of $MnCO_3$, which are in good agreement with the reported $MnCO_3$ [1, 2]. The bands at $\tilde{\nu}$ =1710 and 1620 cm^{-1}, attributed to C=O and C=C vibrations, respectively, indicate the aromatization of glucose during hydrothermal treatment[3]. The bands in the range $\tilde{\nu}$ =1000-1300 cm^{-1}, which include the C-OH stretching and OH bending vibrations, suggest the existence of large numbers of residual hydroxyl groups[3]. C-H stretches were also observed at 2914 cm^{-1} and 2820 cm^{-1} which agree with the reported literatures [4]. These results demonstrate that the resulting sample consisted of $MnCO_3$ and aromatized glucose, and the chemical reactions can be

described as follow[5]:

$$KMnO_4 + RCHO \rightarrow Mn^{2+}(Mn^{3+}) + RCOOH \quad (2)$$

where R presents the groups in glucose molecule excepting for aldehyde group (-CHO). Mn^{7+} can be reduced to Mn^{3+} or Mn^{2+} by glucose in one or two steps, and the aldehyde groups are oxidized to carboxyl groups that can chemically connect with hydroxyl groups in glucose or oxidized glucose molecules through esterification or aromatization reaction[3].

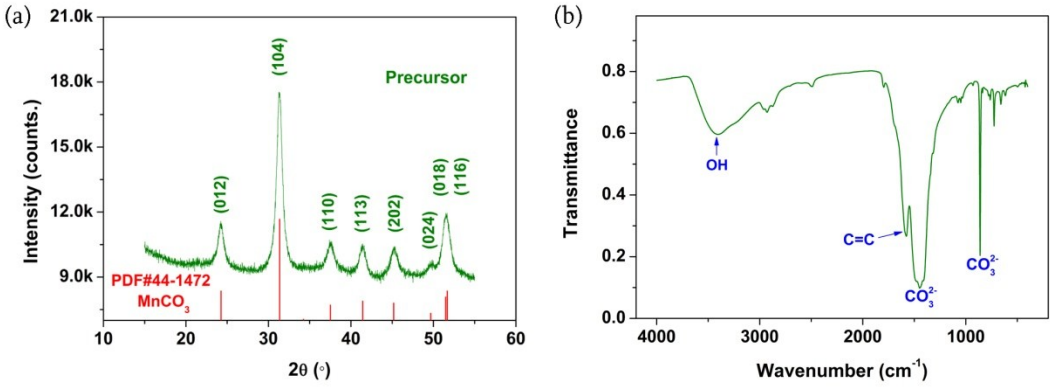

Figure S1. (a) XRD pattern of resulting sample from hydrothermal synthesis and the phase agrees with the characters of $MnCO_3$, indicating $KMnO_4$ and $Mn(CH_3COO)_2$ react to produce Mn(II) compound in the glucose solution. (b) FT-IR spectrum. The vibrations verify the resulting sample consisted of $MnCO_3$ and aromatized glucose.

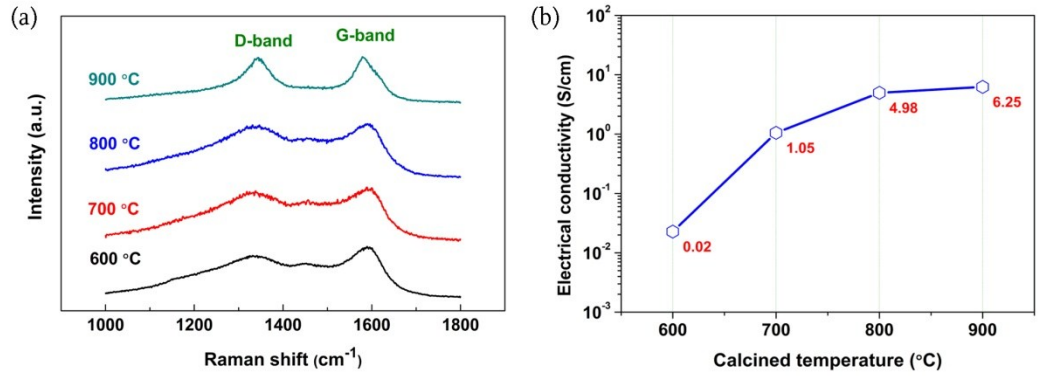

Figure S2. (a) Raman spectra of samples, and the intensity ratios in D- and G-band reveal the enhanced degree of graphitization in carbon. (b) The electrical conductivities in different samples. The higher calcined temperature, the higher electrical conductivity.

All the calcined samples have Type IV curves that indicates the mesopore nature in the samples (Figure S2a), and all surface area exceed 200 m^2/g. While the uncalcined sample show the type III sorption behavior, (Figure S2b) which indicates that the attractive adsorbate-adsorbent interactions are relatively weak[6] and the BET surface area is 29.1 m^2/g, and the pore volume is 0.06 cm^3/g, demonstrating that the spindle-like sample consists of a considerable porosity.

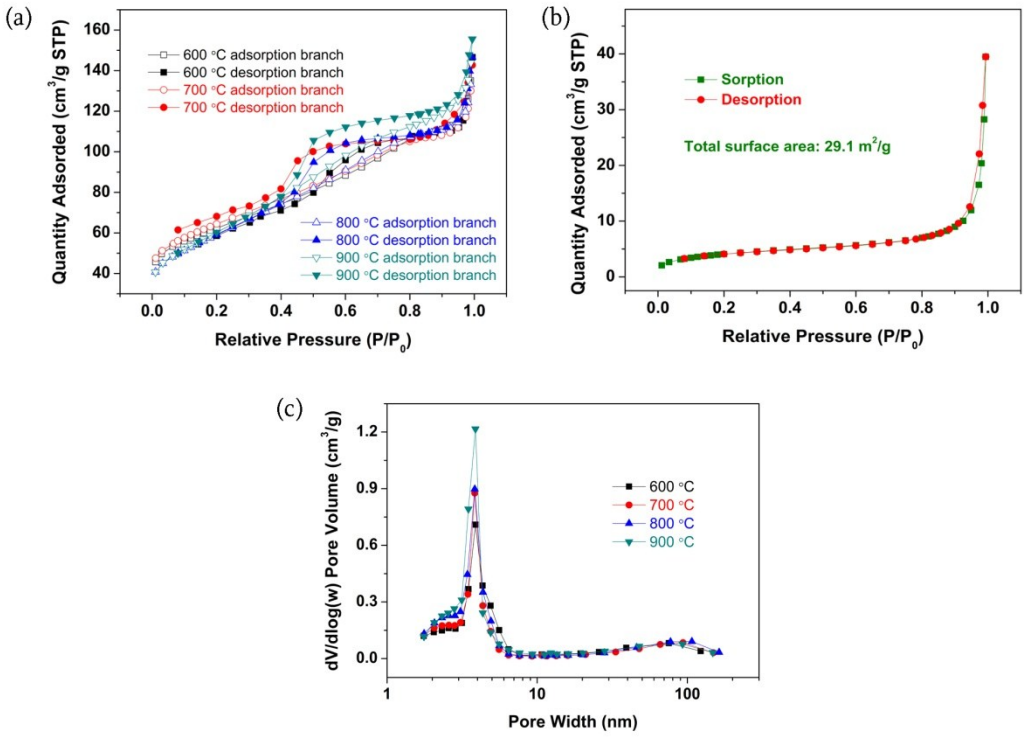

Figure S3. (a) Nitrogen sorption isotherms. (b) Nitrogen sorption isotherm of spindle-like sample before calcinations with a BET surface area of 29.1m^2/g and a pore volume of 0.06 cm^3/g. (c) Pore size distribution of the calcined samples. The pore sizes focus on ~4 nm and the pore volume increases with the elevated calcined temperature.

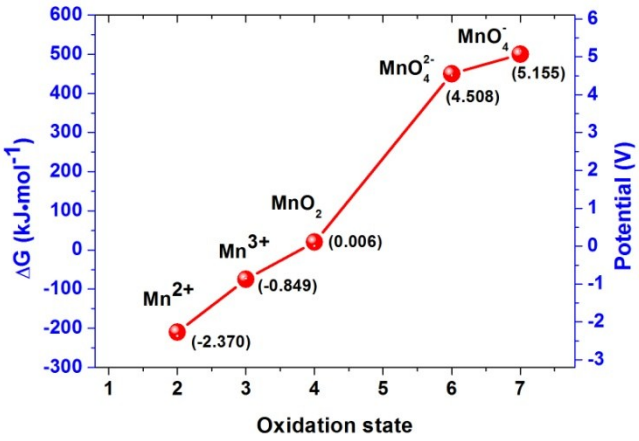

Figure S4. Oxidation state of manganese and corresponding Gibbs free energy and electrochemical potentials. Mn^{2+} has the most stable chemical state because it has the stable electronic configuration ($3d^5$) [7]. Mn^{3+} existed in the resulting sample mainly derived from the incomplete reduction of Mn^{7+} (MnO_4^-) during the synthesis process.

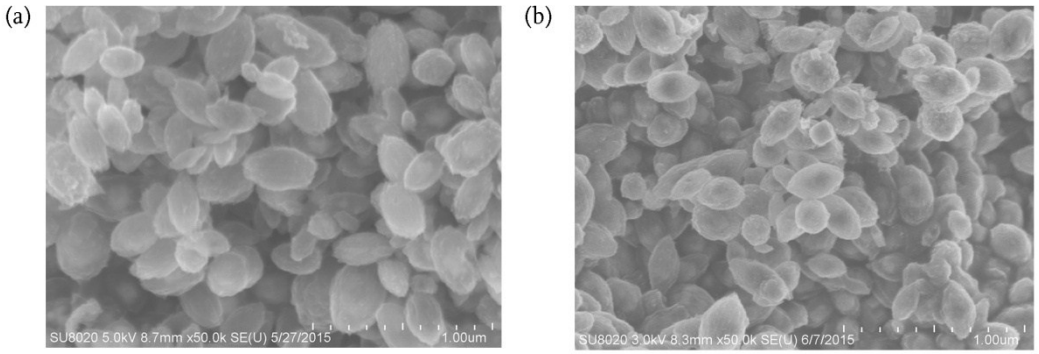

Figure S5. SEM photos show both samples with the spindle-like shape and the sample from 600 °C (a) have bigger sizes in length or width than those in sample from 900 °C (b), implying the higher calcined temperature caused a compact carbon matrix with small shape volume.

Differential scanning calorimetric/ thermogravimetric (DSC/TG) analyses (Figure S6) revealed was two overlapping endothermic peaks located at 400 °C accompanies with the drastic weight loss, indicating the decomposition and pyrolysis of organic complex and $MnCO_3$ [8] occurred in the samples from hydrothermal reaction. Thus, the samples were calcined at temperatures above 600 °C with a flowing nitrogen for guaranteeing the complete pyrolysis.

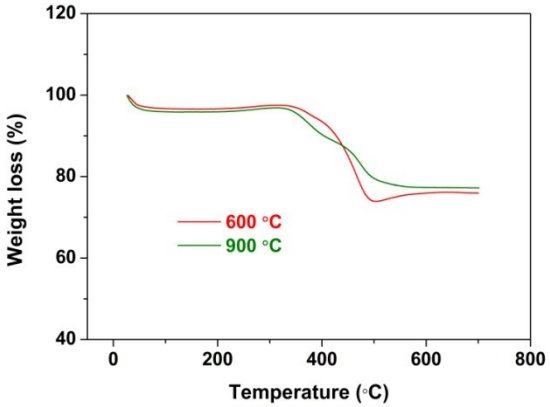

Figure S6. The TG curves of sample 600 and 900 °C measured in flowing oxygen at a rate of 50 ml/min. The carbon content are 25 and 23 *wt*% in sample 600 and 900 °C, respectively. The close carbon content suggests the similar effect on the electrochemical performance in electrodes.

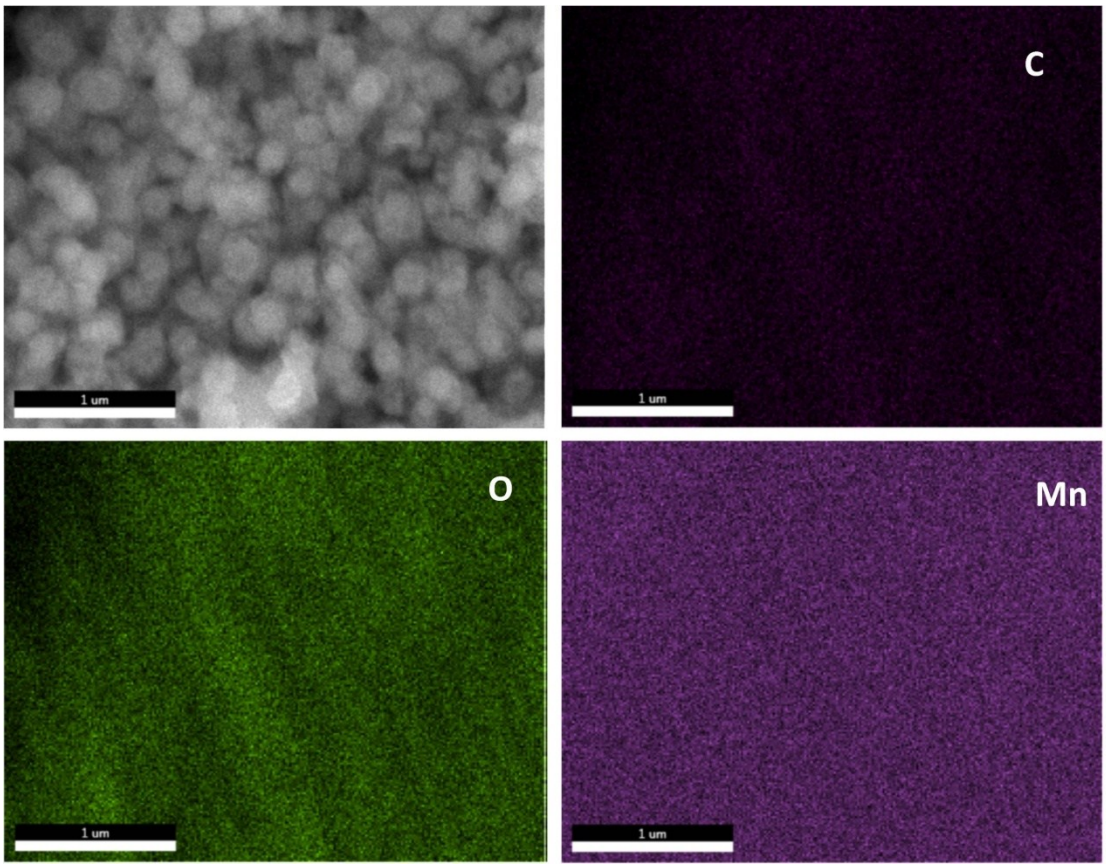

Figure S7. Elements mapping of sample 900 °C. The spindle sample comprised of C, Mn and O agrees with the targeted. Combining to the result from XRD, BET and TEM, it can be concluded that the spindle-like samples are porous carbon encapsulated MnO.

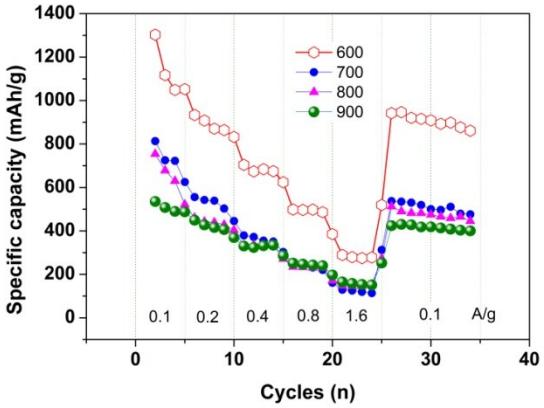

Figure S8. The rate capabilities of all samples. Combining with the cycling stability in Figure 2e, sample 600 °C, remarkably, has the best electrochemical properties. More importantly, sample 600 and 900 °C have the largest differences in electrical conductivity and crystallinity. Therefore, these two samples were chosen as the studying objects and addressed the effects from crystallinity on electrochemical properties.

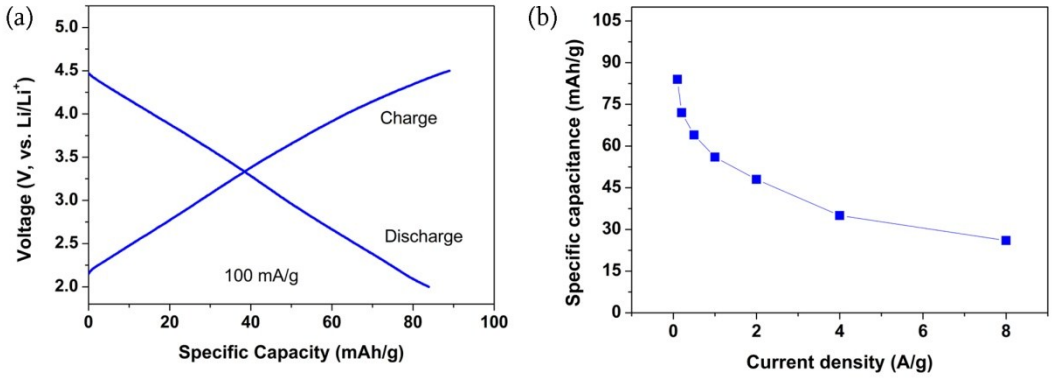

Figure S9. (a) The charge/discharge curves and (b) Rate capability of AC at various current densities in the voltage window of 2-4.5 V. The linear charge or discharge profiles indicate AC in Li in device with an EDLC mechanism to store energy. All data are measured from half-cells where Li metals are used as counter electrodes.

References

1. J. Qu, M. Lu, C. Xu, B. Ding, Y. Zhan, J. Yang and J. Y. Lee, *Nanoscale*, 2014, **6**, 12324-12327.
2. L.-X. Yang, Y. Liang, H. Chen, Y.-F. Meng and W. Jiang, *Mater. Res. Bull.*, 2009, **44**, 1753-1759.
3. X. Sun and Y. Li, *Angew. Chem. Int. Edit*, 2004, **43**, 597-601.
4. J. Gong, L. Luo, S.-H. Yu, H. Qian and L. Fei, *J. Mater. Chem.*, 2006, **16**, 101-105.
5. S. L. Ridgway, *J.Phys. Chem.*, 1930, **35**, 1985-2004.
6. J.-K. Park, *Principles and Applications of Lithium Secondary Batteries*, Wiley-VCH Germany, 2012.
7. G. Xie, L. Yu and Y. Liu, in *Series in Inorganic Chemistry (Vol. IX)*, ed. Q. Zhang, Science Press, 2012, p. 4.
8. K. Ramesh, L. Chen, F. Chen, Z. Zhong, J. Chin, H. Mook and Y.-F. Han, *Catal. Commun.*,

2007, **8**, 1421-1426.